

Formation of millisecond pulsars with wide orbits

Bo Wang,^{1,2,3*} Dongdong Liu,^{1,2,3†} Yunlang Guo,^{4,5‡} Hailiang Chen,^{1,2,3}
Wenshi Tang,^{4,5} Luhan Li^{1,2,3} and Zhanwen Han^{1,2,3}

¹*Yunnan Observatories, Chinese Academy of Sciences, Kunming 650216, China*

²*International Centre of Supernovae, Yunnan Key Laboratory, Kunming 650216, China*

³*University of Chinese Academy of Sciences, Beijing 100049, China*

⁴*School of Astronomy and Space Science, Nanjing University, Nanjing 210023, China*

⁵*Key Laboratory of Modern Astronomy and Astrophysics, Nanjing University, Ministry of Education, Nanjing 210023, China*

Accepted. Received

ABSTRACT

Millisecond pulsars (MSPs) are a kind of radio pulsars with short spin periods, playing a key role in many aspects of stellar astrophysics. In recent years, some more MSPs with wide orbits (> 30 d) have been discovered, but their origin is still highly unclear. In the present work, according to an adiabatic power-law assumption for the mass-transfer process, we carried out a large number of complete binary evolution computations for the formation of MSPs with wide orbits through the iron core-collapse supernova (CCSN) channel, in which a neutron star (NS) originating from a CCSN accretes matter from a red-giant (RG) star and spun up to millisecond periods. We found that this channel can form the observed MSPs with wide orbits in the range of 30 – 1200 d, in which the WD companions have masses in the range of $0.28 - 0.55 M_{\odot}$. We also found that almost all the observed MSPs can be reproduced by this channel in the WD companion mass versus orbital period diagram. We estimate that the Galactic numbers of the resulting MSPs from the CCSN channel are in the range of $\sim 4.8 - 8.5 \times 10^5$. Compared with the accretion-induced collapse channel, the CCSN channel provides a main way to produce MSPs with wide orbits.

Key words: stars: evolution – binaries: close – X-rays: binaries — supernovae: general — stars: neutron

1 INTRODUCTION

Millisecond pulsars (MSPs) are an important subclass of rotation powered radio pulsars with short spin pulse periods (usually < 30 ms) and weak surface magnetic fields ($\sim 10^8 - 10^9$ G), about 80% of which are discovered in binaries (see e.g. Manchester 2004; Lorimer 2008; Han et al. 2021). As the end point of binary evolution, MSPs play a key role in many aspects of stellar astrophysics. The observed stellar and orbital properties of binary MSPs can be used to constrain some important processes during binary evolution, such as the mass-accretion onto neutron stars (NSs), the common-envelope evolution and the angular momentum loss mechanisms, etc (see Tauris 2011; D’Antona & Tailo 2020; Tauris & van den Heuvel 2023). Meanwhile, the exotic evolutionary history and environments combined with the extreme

* E-mail: wangbo@ynao.ac.cn

† E-mail: liudongdong@ynao.ac.cn

‡ E-mail: yunlang@nju.edu.cn

timing stability makes MSPs excellent astrophysics labs to study matter in extreme states (see Bhattacharyya & Roy 2021).

MSPs are believed to be formed from the evolution of low-mass X-ray binaries (LMXBs), where NSs were produced by iron core-collapse supernovae (CCSNe) and have subsequently been spun up to millisecond periods through sufficient mass accretion from their companions, called the standard recycling model (see Alpar et al. 1982; Chanmugam & Brecher 1987; Bhattacharya & van den Heuvel 1991; Podsiadlowski, Rappaport & Pfahl 2002). The recycling model is now widely accepted for the formation of MSPs, but there remain many processes that are not well understood, such as the mass-accretion physics (e.g. accretion efficiency) and the mass-transfer process, etc (see Tauris & van den Heuvel 2006; Tauris 2011). In addition, it has been believed that the accretion-induced collapse (AIC) of oxygen-neon white dwarfs (ONe WDs) will collapse into NSs via electron-capture reactions by Mg and Ne, providing an alternative way to form MSPs (e.g. Ivanova et al. 2008; Hurley et al. 2010; Chen et al. 2011, 2023; Tauris et al. 2013; Freire & Tauris 2014; Guo et al. 2021).

With the development of radio astronomy, more and more MSPs are discovered by the current pulsar surveys based on large radio telescopes, such as the Parkes radio telescope, the Arecibo telescope and the Five-hundred-meter Aperture Spherical radio Telescope (FAST), etc (for a recent review, see Han et al. 2021). Recent observations indicate that some more MSPs with wide separations ($P_{\text{orb}} > 30$ d) are being discovered, but their formation way is still highly unclear (e.g. Cromartie et al. 2016; Bhattacharyya et al. 2019, 2021; Parent et al. 2019; Bondonno et al. 2020; Deneva et al. 2021; Miao et al. 2023; Gautam et al. 2024). Tauris & Savonije (1999) investigated the NS+red-giant (RG) systems to produce MSPs with wide orbits, in which the NSs originating from CCSNe accrete matter from RG donors and spun up to millisecond periods, named as the CCSN channel. However, Tauris & Savonije (1999) did not provide the parameter space for producing MSPs through this channel, and thereby the rate. It is worth noting that Wang, Liu & Chen (2022, Paper I) recently studied the binary computations of ONe WD+RG systems that undergo AIC and then be recycled to form MSPs, called the AIC channel (see also Ablimit 2023). In Paper I, we suggested that the AIC channel could be a viable way to produce MSPs with wide orbits.

In this article, we aim to study the formation of MSPs with long orbital periods through the CCSN channel in a systematic way, and then compare the results with those from the AIC channel. In Section 2, we introduce the numerical code and methods for binary evolution computations of NS+RG systems, and give the corresponding results in Section 3. In Section 4, we present the binary population synthesis (BPS) methods, and provide the rate of MSPs with wide orbits. Finally, a discussion is shown in Section 5 and a summary in Section 6.

2 NUMERICAL CODE AND METHODS

In the CCSN channel, the mass donor is a RG star that transfers H-rich matter and angular momentum onto the surface of the NS, finally forming MSPs with wide orbits. We compute the evolution of NS+RG systems until the formation of binary MSPs by employing the Eggleton stellar evolution code (see Eggleton 1971, 1972, 1973; Han, Podsiadlowski & Eggleton 1994; Pols et al. 1995, 1998). The basic input physics and initial setup for this code are similar to those in Paper I, including the convective overshooting parameter, the mass-transfer process and the NS mass-growth rate, etc. The ratio between mixing length and local pressure scale height is set to be 2.0, and the convective overshooting parameter to be 0.12, approximately corresponding to an overshooting length of ~ 0.25 pressure scale heights (see Pols et al. 1997). A classic Population I composition for the initial main-sequence

models is adopted with H abundance $X = 0.70$, He abundance $Y = 0.28$, and metallicity $Z = 0.02$. In the stellar models, the number of meshpoints is set to be 399. If we set the number of meshpoints to be 199 and 599 for the evolution of NS+RG systems, we found that there is no significant difference in the results. In addition, we did some tests for the influence of the temporal resolution on our results. We also found that there is almost no difference in our results if we change the temporal resolution (for details see Appendix A).

During the Roche-lobe overflow (RLOF), we use an integrated prescription for the mass-transfer process with RG donors, i.e. an adiabatic power-law mass-transfer assumption (see Ge et al. 2010), as follows:

$$\dot{M}_2 = -\frac{2\pi R_L^3}{GM_2} f(q) \int_{\phi_L}^{\phi_s} \Gamma^{1/2} \left(\frac{2}{\Gamma + 1} \right)^{\frac{\Gamma+1}{2(\Gamma-1)}} (\rho P)^{1/2} d\phi, \quad (1)$$

in which \dot{M}_2 is the mass-transfer rate, M_2 is the mass of the donor, G is the gravitational constant, P is the local gas pressure, R_L is the radius of the Roche-lobe, ρ is the local gas density, ϕ_L is the Roche-lobe potential energy ϕ_s is the stellar surface potential energy, and Γ is the adiabatic index. We made more discussions for this mass-transfer process in Section 5.

In our calculations, we do not compute the structure of the NS and suppose it as a point mass, in which we set the initial mass of the NS (M_{NS}^i) as $1.4 M_\odot$ (a canonical NS mass; see van den Heuvel 2009; Chen & Liu 2013). We follow the growth and spin-up of the NS, along with the mass loss of the RG donor and its subsequent evolution to the WD stage. We adopt the prescription of Tauris et al. (2013) to obtain the mass-growth rate of the NS:

$$\dot{M}_{\text{NS}} = (|\dot{M}_2| - \max[|\dot{M}_2| - \dot{M}_{\text{Edd}}, 0]) \cdot k_{\text{def}} \cdot e_{\text{acc}}, \quad (2)$$

in which \dot{M}_{Edd} is the Eddington accretion rate of the NS, k_{def} is the mass ratio of the gravitational mass to the remaining mass of the accreted matter, and e_{acc} is the mass fraction of the transferred matter to the rest on the NS. For H accretion onto the NS, \dot{M}_{Edd} is given by Tauris et al. (2013):

$$\dot{M}_{\text{Edd}} = 4.6 \times 10^{-8} M_\odot \text{ yr}^{-1} \cdot M_{\text{NS}}^{-1/3} \cdot \frac{1}{1 + X_{\text{H}}}, \quad (3)$$

where X_{H} is the H mass fraction of the accreted matter. In this work, k_{def} and e_{acc} are combined into a free parameter $k_{\text{def}} \cdot e_{\text{acc}}$ that represents the mass retention efficiency of the NS. We set $k_{\text{def}} \cdot e_{\text{acc}}$ to be 0.35 on the basis of the increased evidence of the inefficient accretion for LMXBs even though $|\dot{M}_2| < \dot{M}_{\text{Edd}}$ (see, e.g. Jacoby et al. 2005; Antoniadis et al. 2012; Tauris et al. 2013; Ablimit & Li 2015).¹ Accordingly, the NS mass-growth rate can be expressed as:

$$\dot{M}_{\text{NS}} = \begin{cases} 0.35 \dot{M}_2, & |\dot{M}_2| < \dot{M}_{\text{Edd}}, \\ 0.35 \dot{M}_{\text{Edd}}, & |\dot{M}_2| \geq \dot{M}_{\text{Edd}}. \end{cases} \quad (4)$$

During the NS mass-growth process, we suppose that the excess material ($|\dot{M}_2| - \dot{M}_{\text{NS}}$) is ejected from the vicinity of the NS, taking away the specific orbital angular momentum of the accreting NS. For the mass-loss process, we adopted the isotropic re-emission mechanism, in which the excess material was transferred through an accretion disk to the vicinity of the NS, from where it is subsequently ejected in the form of a rapid isotropic wind (see, e.g. Soberman, Phinney & van den Heuvel 1997; Tauris & Savonije 1999). The NS mass-growth

¹ The inefficient accretion may arise from some possible mechanisms, e.g. direct atmosphere irradiation of the donor star from the pulsar, the instabilities of accretion disc, and the propeller effects, etc (see Tauris et al. 2013; see also van Paradijs 1996; Dubus et al. 1999).

Table 1. Summary of some typical NS+RG systems that can evolve into MSPs with different initial donor masses and initial orbital periods, in which we set $M_{\text{NS}}^i = 1.4 M_{\odot}$. The columns (from left to right): the initial donor mass, the initial orbital period; the stellar age at the beginning of RLOF; the time-scale that the binary appears as a LMXB; the final NS mass, the final donor mass (i.e. the WD mass), and the final orbital period; and the minimum spin period of the NS on the basis of equation (5).

Set	M_2^i (M_{\odot})	$\log P_{\text{orb}}^i$ (d)	t_{RLOF} (Gyr)	Δt_{LMXB} (Myr)	M_{NS}^f (M_{\odot})	M_2^f (M_{\odot})	$\log P_{\text{orb}}^f$ (d)	$P_{\text{spin}}^{\text{min}}$ (ms)
1	1.4	0.4	3.438	233	1.7796	0.3000	1.7569	0.70
2	1.4	0.6	3.494	127	1.7600	0.3134	1.9055	0.73
3	1.4	0.8	3.536	102	1.7289	0.3276	2.0531	0.78
4	1.4	1.0	3.568	65	1.7144	0.3434	2.2011	0.81
5	1.4	1.2	3.600	34	1.6395	0.3607	2.3475	0.99
6	1.4	1.4	3.618	17	1.5733	0.3808	2.4980	1.27
7	1.4	1.6	3.621	15	1.5189	0.4036	2.6452	1.68
8	1.4	1.8	3.627	10	1.4825	0.4295	2.7850	2.21
9	1.4	2.0	3.631	7	1.4579	0.4594	2.9174	2.88
10	1.4	2.2	3.634	5	1.4407	0.4955	3.0402	3.75
11	1.1	1.4	8.416	26	1.5956	0.3659	2.3986	1.16
12	1.3	1.4	4.684	23	1.5828	0.3765	2.4723	1.22
13	1.5	1.4	2.874	21	1.5618	0.3848	2.5165	1.33
14	1.7	1.4	1.939	17	1.5361	0.3921	2.5348	1.52
15	1.9	1.4	1.391	13	1.5075	0.3994	2.5316	1.81

rate used in this work is widely adopted in previous studies, see e.g. Ablimit & Li (2015), Liu et al. (2018), Tang, Liu & Wang (2019) and Chen et al. (2021), etc.

The accreted matter will recycle the NS that may undergo the spin-up process (e.g. Li et al. 2021). We calculate the minimum spin period of the recycled NS before the spin-down process based on the prescription of Tauris, Langer & Kramer (2012):

$$P_{\text{spin}}^{\text{min}} \sim 0.34 \times (\Delta M_{\text{NS}}/M_{\odot})^{-3/4}, \quad (5)$$

in which ΔM_{NS} is the mass of the accreted matter onto the NS, and $P_{\text{spin}}^{\text{min}}$ is in units of ms. Here, we neglect the initial spin velocity of the NS and the gravitational binding energy of the accreted matter onto the NS. It is worth noting that Guo et al. (2023) recently explained the formation of the observed isolated mildly recycled pulsars with velocity $< 360 \text{ km s}^{-1}$ on the basis of equation (5).

3 BINARY EVOLUTION RESULTS

In order to form MSPs with wide orbits, we performed a large number of detailed binary evolution computations of NS+RG systems that interact through mass-transfer, and thus we obtain a dense grid of binaries. In Table 1, we show the main evolutionary features of some selected NS+RG systems that can form recycled MSPs. In this table, we explored the effect of different initial orbital periods (see sets 1 – 10) and initial donor masses (see sets 11 – 15) on the final results.

3.1 A representative example for binary evolution

Fig. 1 presents a representative example of the evolution of a NS+RG system that forms a wide-orbit MSP finally (see set 7 in Table 1). The initial binary parameters for this system are $(M_{\text{NS}}^i, M_2^i, \log(P_{\text{orb}}^i/d)) = (1.4, 1.4, 1.6)$, where M_{NS}^i , M_2^i and P_{orb}^i are the initial mass of the NS, the initial mass of the donor, and the initial orbital period, respectively. After about 3.621 Gyr, the donor fills its Roche-lobe owing to the rapid expansion of itself when it

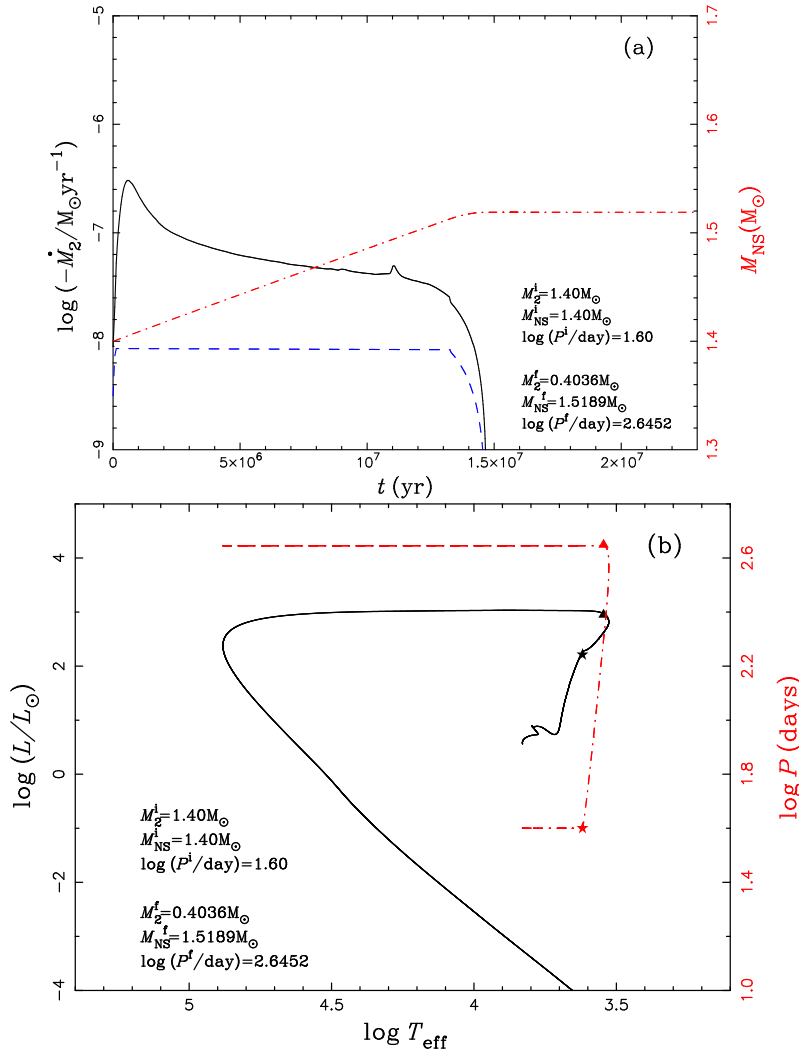


Figure 1. A representative example for the evolution of a NS+RG system until the formation of a recycled MSP, in which $(M_2^i, M_{\text{NS}}^i, \log(P_{\text{orb}}^i/\text{d})) = (1.4, 1.4, 1.6)$ (see set 7 in Table 1). Panel (a): the evolution of the M_{NS} (red dash-dotted line), \dot{M}_2 (black solid line) and \dot{M}_{NS} (blue dashed line) as a function of time for the binary evolution calculations. Panel (b): the binary orbital period (red dash-dotted line) and the luminosity of the mass donor (black solid line) as a function of effective temperature. Asterisks indicate the position where the mass-transfer occurs, whereas triangles mark the position where the mass-transfer stops.

evolves to the RG phase, resulting in a case B mass-transfer process defined by Kippenhahn & Weigert (1967). During this stage, the RG donor contains a convective envelope and transfers H-rich matter onto the NS, leading to a spin-up process for the NS.

The \dot{M}_2 becomes higher than \dot{M}_{Edd} soon after the RLOF. In this case, the NS grows in mass at a rate of $0.35\dot{M}_{\text{Edd}}$, and the majority of the transferred matter is blown away from the system at a rate of $(|\dot{M}_2| - 0.35\dot{M}_{\text{Edd}})$. During the mass-transfer process, the binary shows as a LMXB, lasting for about 15 Myr. At the end of the mass-transfer process, the spin period of the pulsar will approach about 1.68 ms before the spin-down process. After that, the RG donor gradually evolves to a He WD after the exhaustion of its H-shell. The binary forms a long orbital MSP finally, consisting of a $0.4036 M_\odot$ He WD and a $1.5189 M_\odot$ pulsar with an orbital period of about 442 d.

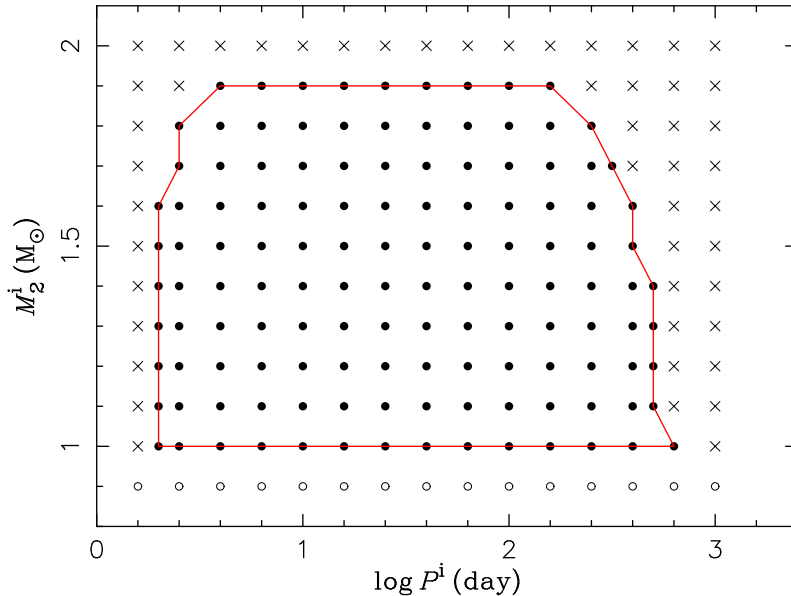


Figure 2. Initial parameter region of NS+RG systems that eventually produce wide orbit MSPs in the $\log P^i - M_2^i$ plane, in which we set $M_{\text{NS}}^i = 1.4 M_{\odot}$. The filled circles indicate systems that lead to the formation of MSPs. The crosses denote systems that will not form MSPs through the CCSN channel, and the open circles are those that the mass donors have stellar age larger than the Hubble time before filling their Roche-lobes.

3.2 Initial parameters of NS+RG systems

Fig. 2 shows the initial parameter space of NS+RG systems that eventually form MSPs in the $\log P^i - M_2^i$ plane with $M_{\text{NS}}^i = 1.4 M_{\odot}$, in which P^i is the initial orbital period of the NS+RG system and M_2^i is the initial mass of the RG donor. In order to form MSPs with wide orbits, the NS+RG systems should have initial orbital periods of $\sim 2 - 600$ d and have RG companions with initial masses of $\sim 1.0 - 1.9 M_{\odot}$. The time-scales that the NS+RG systems appear to be LMXBs range from $\sim 1 - 100$ Myr. In Fig. 2, most of NS+RG systems will evolve to NS+He WD systems. However, some of NS+RG systems with **high-mass** RG donors and long orbital periods will create hot subdwarfs prior to the WD stage, in which the hot subdwarfs will form CO WDs finally (e.g. sets 9 and 10 in Table 1).

The upper boundary of the initial parameter space in Fig. 2 is mainly constrained by a high M_2 due to a large mass-ratio between the RG star and the NS, resulting in the formation of a common-envelope (CE). Systems below the lower boundary have RG donors with stellar age larger than the Hubble time when they fill their Roche-lobes. The left boundary is determined by the shortest orbital periods when the mass donors fill their Roche-lobes at the bottom of the RG phase, whereas the right boundary are constrained by the condition that the mass donors fill their Roche-lobes at the top of the RG phase.

3.3 Resulting MSPs

In Table 2, we listed some relevant parameters of 44 observed MSPs with spin periods < 30 ms detected in the Galactic disk, which have WD companions with orbital periods > 30 d. Fig. 3 shows the resulting binary MSPs formed via the CCSN channel in the final $M_{\text{WD}} - P_{\text{orb}}$ diagram. In this figure, the final binary MSPs follow the well-known relation between M_{WD} and P_{orb} , which can be understood by a relation between the giant's radius and the mass of its degenerate core (see, e.g. Refsdal & Weigert 1971; Rappaport et al. 1995; Tauris & Savonije 1999; Podsiadlowski, Rappaport & Pfahl 2002). From this figure, we can see that the CCSN channel can form binary MSPs with orbital periods in the range

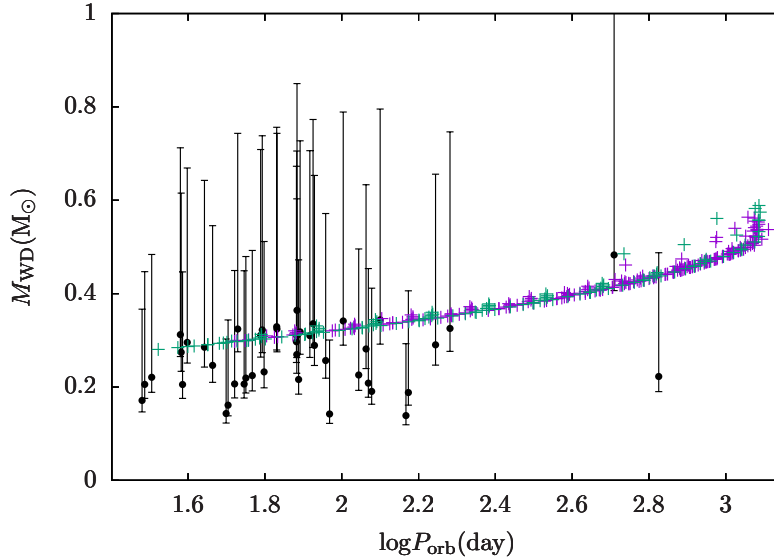


Figure 3. The WD companion masses of the resulting MSPs formed via the CCSN channel as a function of orbital periods (see green crosses). For a comparison, we also show the results for the AIC channel (see purple crosses; see Paper I). The error bars represent the 44 observed MSPs listed in Table 2.

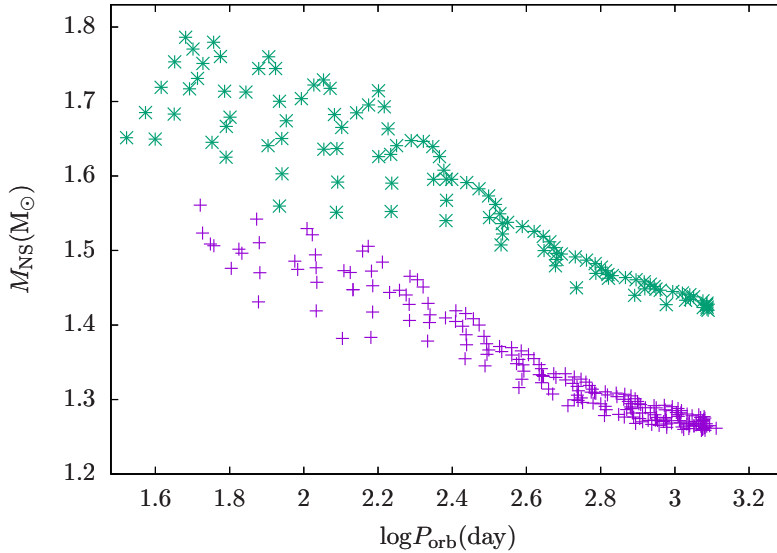


Figure 4. The NS masses of the resulting MSPs formed through the CCSN channel as a function of orbital periods (see green crosses). For a comparison, we also show the results for the AIC channel (see purple crosses; see Paper I).

of 30 – 1200 d, in which the WD companions have masses ranging from $0.28 M_{\odot}$ to $0.55 M_{\odot}$. Almost all the observed MSPs with wide orbits can be reproduced by the CCSN channel in the $M_{\text{WD}} - P_{\text{orb}}$ diagram. It is worth noting that metallicity can influence the radius of RGs and thus the $M_{\text{WD}} - P_{\text{orb}}$ relation. If a lower metallicity is adopted, the $M_{\text{WD}} - P_{\text{orb}}$ relation will be higher than that in Fig. 3, i.e. for a given donor mass the final orbital period at lower metallicity is lower than that at higher metallicity (see, e.g. Tauris & Savonije 1999; Zhang et al. 2021). In addition, the AIC channel can form binary MSPs with orbital periods ranging from 50 d to 1200 d. Compared with the AIC channel, the CCSN channel can produce binary MSPs with shorter orbital periods (~ 30 d) that is mainly decided by the left boundary of the initial parameter space in Fig. 2.

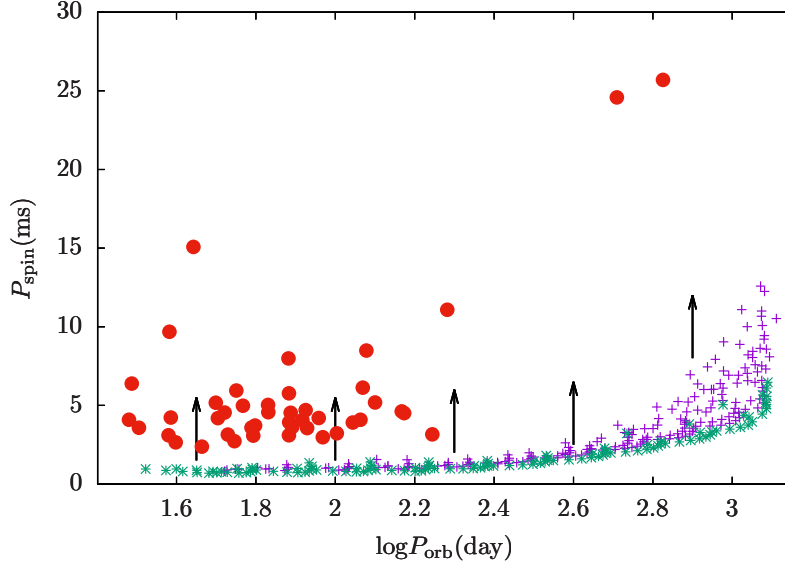


Figure 5. The Corbet diagram for the resulting MSPs on the basis of the CCSN channel (see green crosses). For a comparison, we also show the results for the AIC channel (see purple crosses; Paper I). The filled circles represent the 44 observed MSPs with $P_{\text{spin}} < 30$ ms listed in Table 2. Note that the theoretical models show a lower limit for the pulsar spin, and the direction of the arrows indicates that the spin periods will become longer with the spin-down of the pulsars.

Fig. 4 presents the resulting binary MSPs in the $M_{\text{NS}} - P_{\text{orb}}$ diagram. From this figure, we can see that the final NS masses ranges from $1.42 M_{\odot}$ to $1.79 M_{\odot}$, in which the accreted masses of the recycled pulsars are in the range of $\sim 0.02 - 0.39 M_{\odot}$. For the AIC channel, the final NS masses are in the range of $1.26 M_{\odot}$ to $1.55 M_{\odot}$, in which the accreted masses are in the range of $\sim 0.01 - 0.30 M_{\odot}$ (see Paper I). The final NS masses in the AIC channel are lower than those from the CCSN channel by assuming the same accretion efficiency of a NS. This is because the RG donor in the AIC channel has already lost some of its matter during the pre-AIC evolution, and the NS in the CCSN channel has a larger initial mass (see van den Heuvel 2009). In this figure, we also see that there is an anti-correlation between M_{NS} and P_{orb} for the resulting MSPs, that is, MSPs with wide orbits have lower NS masses. This is because systems with wide orbits have RG donors with larger degenerate cores, leading to less layer matter being transferred onto the NSs. Meanwhile, systems with wide orbits will experience higher mass-transfer process, losing too much matter.

Fig. 5 shows the Corbet diagram for the resulting MSPs on the basis of the CCSN channel. In the present work, the accreted mass for the recycled pulsars is up to $0.4 M_{\odot}$, thus these MSPs will be fully recycled based on equation (5); pulsars with the accreted mass larger than $0.1 M_{\odot}$ are usually known as fully recycled ones (see Tauris et al. 2013). The predicted minimum spin periods for these MSPs range from ~ 1 ms to 15 ms before the spin-down process. With the spin-down of the pulsars, the spin periods will become longer, indicating that the CCSN channel has the potential ability to form the observed MSPs with longer spin periods. If we set the initial spin period of a pulsar as 2 ms (the predicted average spin period in minimum) and its $\dot{P}_{\text{spin}} = 6.26 \times 10^{-20}$, the pulsar needs 1.5 – 3.0 Gyr spin down to 5 ms (the average spin period in observations) by adopting the value of the magnetic braking index as 3 (see Fig. 11 of Tauris, Langer & Kramer 2012). Compared with the AIC channel (see Paper I), the CCSN channel has the lower predicted minimum spin periods for MSPs. This is because the CCSN channel has the larger accreted masses for the recycled pulsars. It is worth noting that there is a significant decrease of MSPs with orbital periods

>200 d in observations. This is mainly due to some observational selection effects for MSPs with wide orbits (for more discussions see Sect. 4.3).

4 BINARY POPULATION SYNTHESIS

4.1 BPS methods

In order to study the Galactic rates of MSPs with wide orbits through the CCSN channel, we performed a series of Monte Carlo BPS simulations on the basis of the Hurley’s rapid binary evolution code (see Hurley, Tout & Pols 2002). The basic initial input and assumptions for Monte Carlo BPS simulations are similar to those in Wang et al. (2021), including the initial mass-ratio distribution, the initial orbital separation distribution and the initial mass function (IMF), etc (for recent reviews on BPS simulations, see e.g. Han et al. 2020; Chen, Liu & Han 2024). The following basic assumptions are adopted:

(1) We assume that all stars are produced in the form of binaries from zero-age main-sequence (i.e. primordial binaries), in which a circular orbit is set.

(2) A constant mass-ratio distribution is supposed for primordial binaries,

$$n(q) = 1, \quad 0 < q \leq 1, \quad (6)$$

in which $q = M_{2,i}/M_{1,i}$, where $M_{1,i}$ and $M_{2,i}$ are the initial masses of the primordial primary and secondary, respectively (see Mazeh et al. 1992; Goldberg & Mazeh 1994; Shatsky & Tokovinin 2002).

(3) We supposed the orbital separation distribution as constant in $\log a$ for primordial binaries with wide orbits, where a is the orbital separation of the primordial binary.

(4) Since the MSP progenitor comes from massive stars, we adopt the IMF of Kroupa (2001) for the primordial primaries, in which $M_{1,i}$ ranges from $0.1 M_{\odot}$ to $100 M_{\odot}$.

(5) We adopt a constant star formation rate over the last 15 Gyr, where we assume that a primordial binary with its primary $> 0.8 M_{\odot}$ is produced every year (see Han, Podsiadlowski & Eggleton 1995; Hurley, Tout & Pols 2002). According to this calibration, we can obtain a constant star formation rate of $\sim 5 M_{\odot} \text{yr}^{-1}$ (see Willems & Kolb 2004).

In each simulation, we follow the evolution of a sample of 1×10^7 binaries from primordial binaries until the production of NS+RG systems based on a binary evolutionary way (see Sect. 4.2), in which we did not consider the contribution of the AIC channel to NS+RG systems. A MSP with a wide orbit is assumed to be formed once the initial binary parameters of a NS+RG system are located in the initial parameter space of Fig. 2. It is worth noting that MSPs probably emerge from the evolution of CE in giant binaries. Accordingly, we adopt the standard energy prescription to obtain the output of the CE evolution (see Webbink 1984). As in previous studies (see e.g. Wang et al. 2009, 2021), we combine the stellar structure parameter (λ) and the CE ejection efficiency (α_{CE}) into a free parameter (i.e. $\alpha_{\text{CE}}\lambda$). In order to explore the effect of different values of $\alpha_{\text{CE}}\lambda$ on the final results, we set $\alpha_{\text{CE}}\lambda = 1.0$ and 1.5 for a comparison.

4.2 Evolutionary way to NS+RG systems

According to the evolutionary stage of the primordial primary (i.e. the progenitor of the NS) at the beginning of the first RLOF, there is one binary evolutionary way that can produce NS+RG systems and then form MSPs with wide orbits (see Fig. 6). The primordial primary first fills its Roche-lobe at the early asymptotic giant branch (EAGB) stage. In this case, the mass-transfer is dynamically unstable due to the large mass-ratio and a CE will be formed.

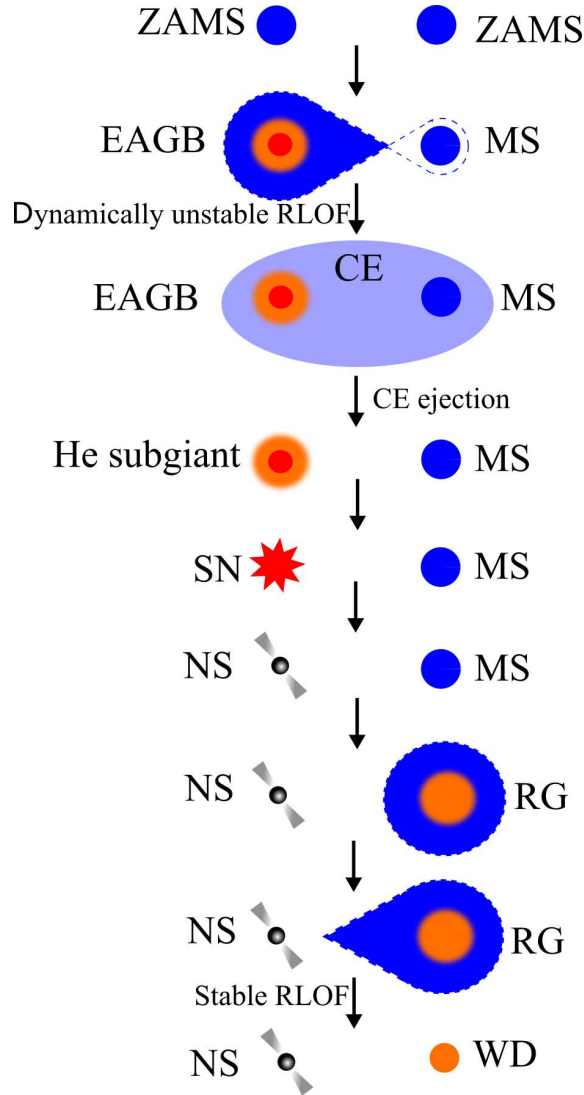


Figure 6. Binary evolutionary way to NS+RG systems that can form MSPs with wide orbits.

If the CE can be ejected, the primordial primary becomes a He subgiant star (a He star at the Hertzsprung gap stage; see Hurley, Tout & Pols 2002), and then the binary continues to evolve. The He subgiant star continues to evolve, leading to the formation of a NS via a CCSN. A NS+RG system will be formed when the primordial secondary evolves to be a RG star. When the RG star fills its Roche-lobe, the binary behaves as a LMXB. After the mass-transfer process, a MSP with a He WD companion will be produced. In some cases, the mass donors will create hot subdwarfs prior to the WD stage, finally forming CO WDs (see Sect. 3.2). For this channel, the initial parameters of the primordial binaries for producing wide-orbit MSPs are in the range of $M_{1,i} \sim 10 - 20 M_{\odot}$, $q = M_{2,i}/M_{1,i} < 0.2$, and $P^i \sim 600 - 3800$ days, where q and P^i are the primordial mass ratio and the initial orbital period, respectively.

4.3 BPS results

Table 3 presents the estimated Galactic rates and numbers of the resulting MSPs with wide orbits, in which we compare the results between the CCSN and AIC channels with different

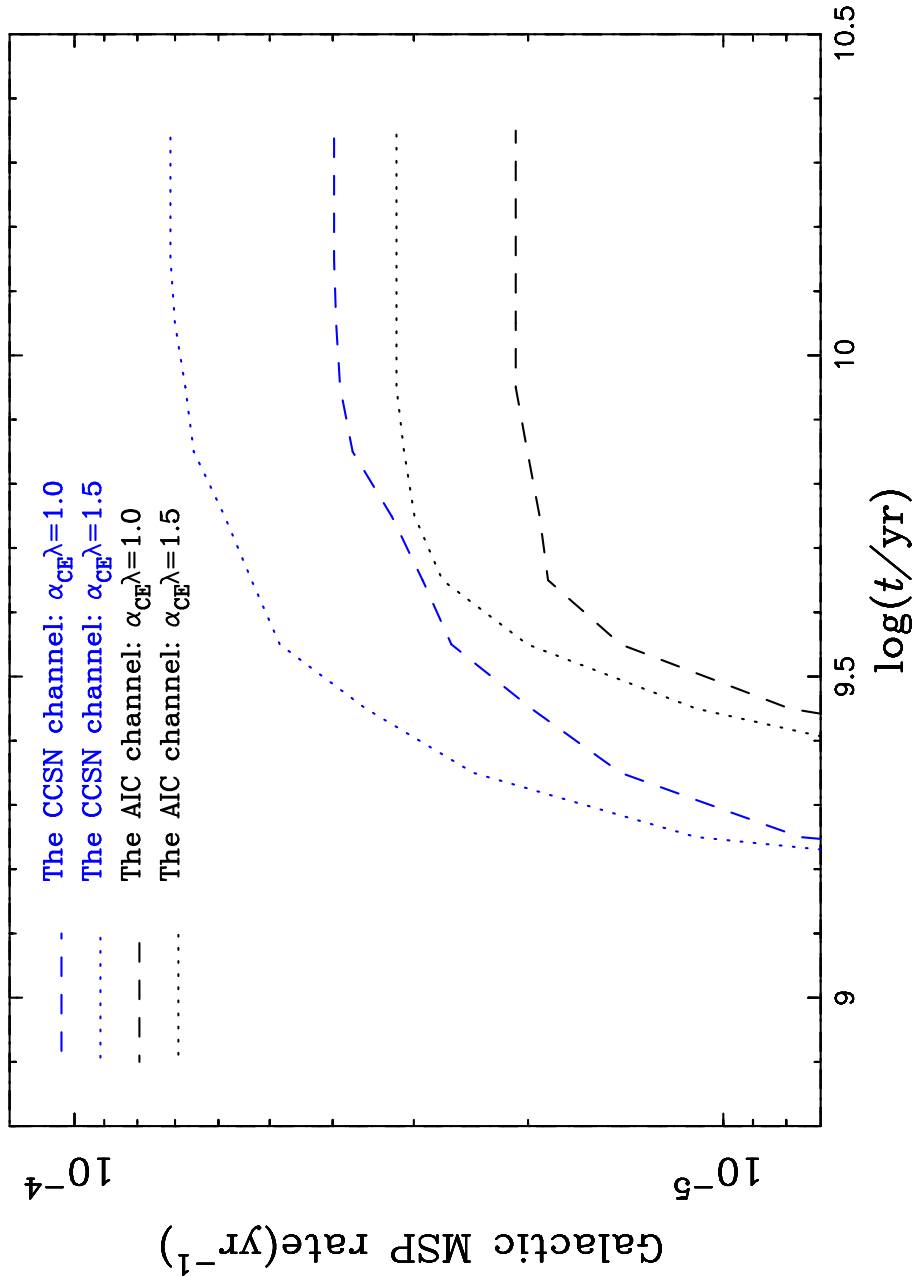


Figure 7. Evolution of the Galactic rates of MSPs from the CCSN channel as a function of time by adopting metallicity $Z = 0.02$ and a constant star formation rate of $5 M_{\odot}\text{yr}^{-1}$. For a comparison, we also show the results for the AIC channel.

CE ejection parameters. For the AIC channel, we obtain the BPS results based on Fig. 3 in Paper I.

Fig. 7 shows the evolution of the Galactic rates of MSPs from the CCSN channel by adopting a constant star formation rate of $5 M_{\odot}\text{yr}^{-1}$. The simulations give the Galactic rates of MSPs from the CCSN channel to be $\sim 4.0 - 7.1 \times 10^{-5} \text{yr}^{-1}$, and the numbers of the resulting MSPs are $\sim 4.8 - 8.5 \times 10^5$ in the Galaxy. In Fig. 7, we set an initial Population I composition ($Z = 0.02$) for the binary evolution computations. If we adopt a lower value of metallicity, the initial region forming MSPs in Fig. 2 will move to shorter orbital periods and lower masses of companions, resulting a lower Galactic rates of MSPs (see, e.g. Meng, Chen & Han 2009; Wang & Han 2010). It is worth noting that the predicted number of Galactic wide-orbit MSPs is much higher than these in observations. This is mainly due to

some observational selection effects, as follows: (1) It is hard to observe MSPs with long orbital periods (see Wang et al. 2020). (2) We can only detect these pulsars, whose radiated beams of light orientate themselves towards us. (3) These observations that only detected 44 wide-orbit MSPs in the Galactic disk (see Table 2) have their only selection effects, such as the detection limit of radio luminosity and the observational area, etc. Therefore, it is hard to directly compare our predictions with these in observations.

In Fig. 7, we also show the results of the AIC channel for a comparison. According to the AIC channel, the predicted Galactic rates of MSPs with wide orbits are $\sim 2.1 - 3.2 \times 10^{-5} \text{ yr}^{-1}$, and the numbers of the resulting MSPs are in the range of $\sim 2.5 - 3.8 \times 10^5$ in the Galaxy (see Paper I; Wang 2018). Compared with the AIC channel, the CCSN channel plays a main way to produce MSPs with wide separations. From this figure, we can see that the estimated Galactic rates of MSPs are strongly dependent on the value of the CE ejection parameter $\alpha_{\text{CE}}\lambda$. However, the CE ejection parameter is still highly uncertain (e.g. Nelemans & Tout 2005; Ivanova et al. 2013). Note that α_{CE} and/or λ might be lower than 1 as several studies suggested (see, e.g. Dewi & Tauris 2000; Scherbak & Fuller 2023). If we adopt a lower value of $\alpha_{\text{CE}}\lambda$ (e.g. 0.5), the Galactic rates of MSPs from the CCSN and AIC channels will decrease to $\sim 1.7 \times 10^{-5} \text{ yr}^{-1}$ and $\sim 1.9 \times 10^{-5} \text{ yr}^{-1}$, respectively.

5 DISCUSSION

Previous investigations usually adopted a surface boundary criteria to deal with the mass-transfer process once the donor star fills its Roche-lobe, as follows:

$$\dot{M}_2 = -C \max[0, (\frac{R_2}{R_L} - 1)^3], \quad (7)$$

in which R_2 is the donor radius, R_L is the radius of its Roche-lobe, and C is a dimensionless constant usually assumed to be $1000 \text{ M}_\odot \text{ yr}^{-1}$ (e.g. Han, Tout & Eggleton 2000; Wang & Han 2010). On the basis of this assumption, the exceeding mass of the donor would be transferred onto the surface of the accretor when the RLOF happens. It has been suggested that the constant C in equation (7) is too large for semidetached binaries with giant donors, likely overestimating the mass-transfer rate (see Liu et al. 2019, and references therein).

In this work, by assuming that the state equation for RG donors follows an adiabatic power law, and that the mass outflow is laminar and occurs along the equipotential surface, we adopted an approximate criterion for the process of the mass-transfer, see equation (1). In this prescription, the \dot{M}_2 changes with the local matter states, corresponding to a variable C in equation (7). Meanwhile, the \dot{M}_2 for RG donors will be lower than that in equation (7), leading to a lower mass-loss rate, and thus more matter will be accumulated onto the NS. It has been argued that the birthrate of type Ia SNe from the semidetached symbiotic channel with RG donors is relatively low (see, e.g. Li & van den Heuvel 1997; Han & Podsiadlowski 2004). By using this mass-transfer assumption, however, Liu et al. (2019) recently enlarged the parameter space for producing type Ia SNe significantly based on the semidetached symbiotic channel. It is worth noting that the integrated mass-transfer assumption for RG donors is still an open question. Woods & Ivanova (2011) argued that a RG star will not expand adiabatically when the local thermal timescale of the superadiabatic outer surface is comparable with the mass-loss timescale. This implies that this work might underestimate the mass-transfer rate, but at least we provide an upper limit of the initial parameter space forming binary MSPs with wide separations.

In the present work, we only consider the formation of binary MSPs in the Galactic disk. In the dense globular clusters, however, MSPs with wide orbits can be formed through

isolated pulsars that have captured WDs (see, e.g. Verbunt & Freire 2014). Meanwhile, the AIC channel could produce newborn pulsars with small kicks, and thus this channel can be used to explain obviously young pulsars in some globular clusters (see, e.g. Boyles et al. 2011). It is worth noting that the AIC channel may help to solve the observed discrepancy between the large rate of MSPs and the small rate of LMXBs in the Galaxy (see, e.g. Kulkarni & Narayan 1988; Bailyn & Grindlay 1990; Tauris et al. 2013). For a recent review on the formation of MSPs through the AIC channel, see Wang & Liu (2020).

In the observations, NSs with RG donors can be identified as symbiotic X-ray binaries that are a rare class of LMXBs. They can also show as ultraluminous X-ray sources during high mass-transfer stage (see, e.g. Shao & Li 2015; Misra et al. 2020). There are several observed symbiotic X-ray binaries that consist of pulsars and RG donors, as follows: (1) V2116 Oph (i.e. GX 1+4) has a pulsar with an orbital period of ~ 1161 d, in which the pulsar with a spin period of ~ 2 min (see, e.g. Hinkle et al. 2006; Īkiewicz, Mikołajewska & Monard 2017). Hinkle et al. (2006) suggested that the maximum mass of the RG donor is about $1.22 M_{\odot}$ by adopting a NS mass of $1.35 M_{\odot}$. (2) V934 Her (i.e. 4U 1700+24) has a pulsar with an orbital period of ~ 12 yr, in which the observed properties of the pulsar are driven by mass accretion from the RG via stellar wind (see, e.g. Hinkle et al. 2019). (3) SRGA J181414.6-225604 is an unique case of a symbiotic X-ray system, in which the steady wind-accretion leads to faint X-ray emission as the orbit is wide enough (see De et al. 2023). (4) IGR J17329-2731 has a highly magnetized NS that accretes material via the stellar wind from its giant companion (see Bozzo et al. 2018). (5) It has been suggested that IGR J16194-2810 is a symbiotic X-ray binary with an orbital period of ~ 193 d, consisting of a $1.23^{+0.05}_{-0.03} M_{\odot}$ NS and a giant mass of $0.99^{+0.02}_{-0.03} M_{\odot}$ (see Hinkle et al. 2024; Nagarajan et al. 2024). In future observations, more symbiotic X-ray binaries are expected to test the theoretical models in this work.

6 SUMMARY

In this work, by employing an adiabatic power-law assumption for the mass-transfer process, we performed a large number of complete binary evolution calculations for the formation of MSPs with wide orbits through the CCSN channel in a systematic way. We found that the CCSN channel can form MSPs with orbital periods ranging from 30 d to 1200 d, in which the masses of the WD companions are in the range of $0.28 - 0.55 M_{\odot}$. We also found that there exists an anti-correlation between the final NS mass and orbital period, and that all the final MSPs through the CCSN channel follow the correlation between the companion mass and the orbital period. In the observations, NSs with RG donors can be identified as LMXBs lasting for $\sim 1 - 100$ Myr. By using a detailed BPS approach, we estimate the numbers of the resulting MSPs in the range of $\sim 4.8 - 8.5 \times 10^5$ in the Galaxy. Compared with the AIC channel, the CCSN channel provides a main way to explain the observed MSPs with wide separations, especially in the Galactic disk. More observational identifications and theoretical simulations on MSPs with wide orbits are needed for our understanding of this class of wide compact systems.

ACKNOWLEDGMENTS

We acknowledge the anonymous referee for valuable comments that help to improve the paper. This study is supported by the National Natural Science Foundation of China (Nos

12225304, 12073071, 12273105, 12288102, 12090040, 12090043), the National Key R&D Program of China (Nos 2021YFA1600404), the Western Light Project of CAS (No. XBZG-ZDSYS-202117), the Youth Innovation Promotion Association CAS (No. 2021058), the science research grants from the China Manned Space Project (Nos CMS-CSST-2021-A12/A10), the Frontier Scientific Research Program of Deep Space Exploration Laboratory (No. 2022-QYKYJH-ZYTS-016), the Yunnan Fundamental Research Projects (Nos 202401AV070006, 202101AT070027, 202101AW070003, 202201AW070011, 202201BC070003), and the Yunnan Revitalization Talent Support Program (Yunling Scholar Project and Young Talent Project).

DATA AVAILABILITY

The data of the numerical calculations can be available by contacting BW.

REFERENCES

- Ablimit I., 2023, MNRAS, 519, 1327
 Ablimit I., Li X.-D., 2015, ApJ, 800, 98
 Alpar M. A., Cheng A. F., Ruderman M. A., Shaham J., 1982, Nature, 300, 728
 Antoniadis J. et al., 2012, MNRAS, 423, 3316
 Bailyn C. D., Grindlay J. E., 1990, ApJ, 353, 159
 Bozzo E. et al., 2018, A&A, 613, A22
 Bhattacharya D., van den Heuvel E. P. J., 1991, PhR, 203, 1
 Bhattacharyya B. et al., 2019, ApJ, 881, 59
 Bhattacharyya B. et al., 2021, ApJ, 910, 160
 Bhattacharyya B., Roy J., 2021, arXiv:2104.02294
 Bondonneau L. et al., 2020, A&A, 635, A76
 Boyles J. et al., 2011, ApJ, 742, 51
 Chanmugam G., Brecher K., 1987, Nature, 329, 696
 Chen H.-L., Tauris T. M., Chen X., Han Z., 2023, ApJ, 951, 91
 Chen H.-L., Tauris T. M., Han Z., Chen X., 2021, MNRAS, 503, 3540
 Chen W.-C., Liu W.-M., 2013, MNRAS, 432, L75
 Chen W.-C., Liu X.-W., Xu R.-X., Li X.-D., 2011, MNRAS, 410, 1441
 Chen X., Liu Z., Han Z., 2024, PrPNP, 134, 104083
 Cromartie H. T. et al., 2016, ApJ, 819, 34
 D’Antona F., Tailo M., 2020, arXiv:2011.11385
 De K. et al., 2022, ApJ, 935, 36
 Deneva J. S. et al., 2021, ApJ, 909, 6
 Dewi J. D. M., Tauris T. M., 2000, A&A, 360, 1043
 Dubus G., Lasota J.-P., Hameury J.-M., Charles P., 1999, MNRAS, 303, 139
 Eggleton P. P., 1971, MNRAS, 151, 351
 Eggleton P. P., 1972, MNRAS, 156, 361
 Eggleton P. P., 1973, MNRAS, 163, 279
 Freire P. C. C., Tauris T. M., 2014, MNRAS, 438, L86
 Gautam T. et al., 2024, A&A, 682, A103
 Ge H., Hjellming M. S., Webbingk R. F., Chen X., Han Z., 2010, ApJ, 717, 724
 Goldberg D., Mazeh T., 1994, A&A, 282, 801
 Guo Y., Liu D., Wu C., Wang B., 2021, RAA, 21, 034
 Guo Y., Wang B., Wu C., Chen W., Jiang L., Han Z., 2023, MNRAS, 526, 932

- Han J. L. et al., 2021, *Res. Astron. Astrophys.*, 21, 107
- Han Z., Ge H., Chen X., Chen H., 2020, *Res. Astron. Astrophys.*, 20, 161
- Han Z., Podsiadlowski Ph., 2004, *MNRAS*, 350, 1301
- Han Z., Podsiadlowski Ph., Eggleton P. P., 1994, *MNRAS*, 270, 121
- Han Z., Podsiadlowski P., Eggleton P. P., 1995, *MNRAS*, 272, 800
- Han Z., Tout C. A., Eggleton P. P., 2000, *MNRAS*, 319, 215
- Hinkle K. H. et al., 2006, *ApJ*, 641, 479
- Hinkle K. H., et al., 2024, *ApJ*, in press (arXiv:2405.02270)
- Hinkle K. H., Fekel F. C., Joyce R. R., Mikołajewska J., Gałan C., Lebzelter T., 2019, *ApJ*, 872, 43
- Hurley J. R., Tout C. A., Pols O. R., 2002, *MNRAS*, 329, 897
- Hurley J. R., Tout C. A., Wickramasinghe D. T., Ferrario L., Kiel P. D., 2010, *MNRAS*, 402, 1437
- Iben I., Tutukov A. V., 1986, *ApJ*, 311, 742
- Ikiewicz K., Mikołajewska J., Monard B., 2017, *A&A*, 601, A105
- Ivanova N., Heinke C. O., Rasio F. A., Belczynski K., Fregeau J. M., 2008, *MNRAS*, 386, 553
- Jacoby B. A., Hotan A., Bailes M., Ord S., Kulkarni S. R., 2005, *ApJ*, 629, L113
- Kippenhahn R., Weigert A., 1967, *Z. Ap.*, 65, 251
- Kroupa P., 2001, *MNRAS*, 322, 231
- Kulkarni S. R., Narayan R., 1988, *ApJ*, 335, 755
- Li X.-D., van den Heuvel E. P. J., 1997, *A&A*, 322, L9
- Li Z., Chen X., Chen H.-L., Han Z., 2021, *ApJ*, 922, 158
- Liu D., Wang B., Chen W., Zuo Z., Han Z., 2018, *MNRAS*, 477, 384
- Liu D., Wang B., Ge H., Chen X., Han Z., 2019, *A&A*, 622, A35
- Lorimer D. R., 2008, *LRR*, 11, 8
- Manchester R. N., 2004, *Science*, 304, 542
- Manchester R. N., Hobbs G. B., Teoh A., Hobbs M., 2005, *AJ*, 129, 1993
- Mazeh T., Goldberg D., Duquennoy A., Mayor M., 1992, *ApJ*, 401, 265
- Meng X., Chen X., Han Z., 2009, *MNRAS*, 395, 2103
- Miao C. C. et al., 2023, *MNRAS*, 518, 1672
- Misra D., Fragos T., Tauris T. M., Zapartas E., Aguilera-Dena D. R., 2020, *A&A*, 642, A174
- Nagarajan P., El-Badry K., Lam C., Reggiani H., 2024, *PASP*, in press (arXiv:2405.17560)
- Nelemans G., Tout C. A., 2005, *MNRAS*, 356, 753
- Parent E. et al., 2019, *ApJ*, 886, 148
- Podsiadlowski Ph., Rappaport S., Pfahl E. D., 2002, *ApJ*, 565, 1107
- Pols O. R., Schröder K. P., Hurly J. R., Tout C. A., Eggleton P. P., 1998, *MNRAS*, 298, 525
- Pols O. R., Tout C. A., Eggleton P. P., Han Z., 1995, *MNRAS*, 274, 964
- Pols O. R., Tout C. A., Schröder K. P., Eggleton P. P., Manners J., 1997, *MNRAS*, 289, 869
- Refsdal S., Weigert A., 1971, *A&A*, 13, 367
- Rappaport S., Podsiadlowski P., Joss P. C., Di Stefano R., Han Z., 1995, *MNRAS*, 273, 731
- Scherbak P., Fuller J., 2023, *MNRAS*, 518, 3966
- Shao Y., Li X.-D., 2015, *ApJ*, 802, 131
- Shatsky N., Tokovinin A., 2002, *A&A*, 382, 92
- Soberman G. E., Phinney E. S., van den Heuvel E. P. J., 1997, *A&A*, 327, 620

- Tang W., Liu D., Wang B., 2019, MNRAS, 490, 752
Tauris T. M., 2011, ASPC, 447, 285
Tauris T. M., Langer N., Kramer M., 2012, MNRAS, 425, 1601
Tauris T. M., Sanyal D., Yoon S.-C., Langer N., 2013, A&A, 558, A39
Tauris T. M., Savonije G. J., 1999, A&A, 350, 928
Tauris T. M., van den Heuvel E. P. J., 2006, in Lewin W. H. G., van der Klis M., eds, Compact Stellar X-ray Sources. Cambridge Univ. Press, Cambridge, p. 623
Tauris T. M., van den Heuvel E. P. J., 2023, Physics of Binary Star Evolution: From Stars to X-ray Binaries and Gravitational Wave Sources, Princeton Univ. Press
van den Heuvel E. P. J., 2009, in Astrophysics and Space Science Library, 359, Physics of Relativistic Objects in Compact Binaries: From Birth to Coalescence, eds. Colpi M., Casella P., Gorini V., Moschella U., Possenti A., (Berlin: Springer-Verlag), 125
van Paradijs J., 1996, ApJ, 464, L139
Verbunt F., Freire P. C. C., 2014, A&A, 561, A11
Wang B., 2018, MNRAS, 481, 439
Wang B., Chen W., Liu D., Chen H., Wu C., Tang W., Guo Y., Han Z., 2021, MNRAS, 506, 4654
Wang B., Chen X., Meng X., Han Z., 2009, ApJ, 701, 1540
Wang B., Han Z., 2010, A&A, 515, A88
Wang B., Liu D., 2020, Res. Astron. Astrophys., 20, 135
Wang B., Liu D., Chen H., 2022, MNRAS, 510, 6011 (Paper I)
Wang L. et al., 2020, ApJ, 892, 43
Webbink R. F., 1984, ApJ, 277, 355
Willems B., Kolb U., 2004, A&A, 419, 1057
Woods T. E., Ivanova N., 2011, ApJL, 739, L48
Zhang Y., Chen H., Chen X., Han Z., 2021, MNRAS, 502, 383

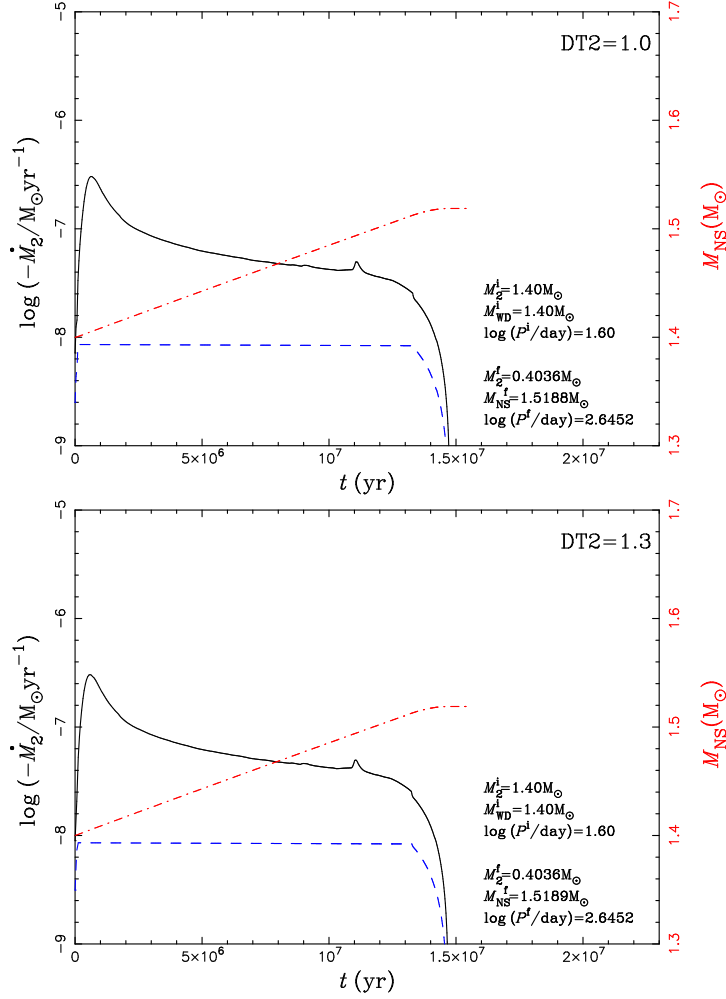


Figure A1. Similar to Panel (a) of Fig. 1, but for $DT2 = 1.0$ and 1.3 .

APPENDIX A: THE TEMPORAL RESOLUTION

In the Eggleton stellar evolution code, in order to prevent the timestep from fluctuating too rapidly, the ratio between the next timestep and the present timestep is restricted to lie in the range $(DT1, DT2)$, where the $DT1$ is usually set to be in the range of $0.8 - 1.0$ and $DT2 = 1.0 - 1.2$. If both $DT1$ and $DT2$ are 1, then the timestep is constant.

In this work, we set $DT1 = 0.8$ and $DT2 = 1.2$ for our binary evolution calculations. In this appendix, we made some tests for the influence of the temporal resolution on our results. In our tests, the initial binary parameters are similar to those in Fig. 1, i.e. $(M_{NS}^i, M_2^i, \log(P_{orb}^i/d)) = (1.4, 1.4, 1.6)$, but we set $DT2 = 1.0$ and 1.3 (see Fig. A1). From Fig. A1, we can see that there is almost no difference in our results when we change the values of $DT2$.

Table 2. The relevant parameters of 44 observed MSPs with $P_{\text{spin}} < 30$ ms detected in the Galactic disk, which have WD companions with wide orbits ($P_{\text{orb}} > 30$ d). The observed data are taken from the ATNF Pulsar Catalogue in January 2024 (see <http://www.atnf.csiro.au/research/pulsar/psrcat>; see Manchester et al. 2005). The median WD masses are calculated by assuming an orbital inclination angle of 60° and a pulsar mass of $1.35 M_\odot$. The error bars of the WD masses for the lower limit correspond to an inclination angle of 90° , and the upper limit marks a 90% probability.

No.	Pulsars	P_{spin} (ms)	\dot{P}_{spin}	P_{orb} (d)	M_{WD} (M_\odot)
1	J0203 – 0150	5.17	1.4e-20	50.0	$0.14^{+0.16}_{-0.02}$
2	J0214 + 5222	24.58	3.0e-19	512.0	$0.48^{+0.70}_{-0.07}$
3	J0407 + 1607	25.70	7.9e-20	669.1	$0.22^{+0.27}_{-0.03}$
4	J0605 + 3757	2.73	4.8e-21	55.7	$0.32^{+0.24}_{-0.03}$
5	J0614 – 3329	3.15	1.8e-20	53.6	$0.32^{+0.42}_{-0.05}$
6	J0732 + 2314	4.09	6.0e-21	30.2	$0.17^{+0.20}_{-0.02}$
7	J0921 – 5202	9.68	1.7e-20	38.2	$0.27^{+0.34}_{-0.04}$
8	J1012 – 4235	3.10	*	38.0	$0.31^{+0.40}_{-0.05}$
9	J1125 – 5825	3.10	6.1e-20	76.4	$0.31^{+0.40}_{-0.05}$
10	J1146 – 6610	3.72	0.8e-20	62.8	$0.23^{+0.28}_{-0.03}$
11	J1312 + 0051	4.23	1.8e-20	38.5	$0.21^{+0.24}_{-0.03}$
12	J1421 – 4409	6.39	1.2e-20	30.7	$0.21^{+0.24}_{-0.03}$
13	J1455 – 3330	7.99	2.4e-20	76.2	$0.30^{+0.38}_{-0.04}$
14	J1529 – 3828	8.49	2.7e-20	119.7	$0.19^{+0.22}_{-0.03}$
15	J1536 – 4948	3.08	2.1e-20	62.1	$0.32^{+0.42}_{-0.05}$
16	J1623 – 2631	11.08	6.7e-19	191.4	$0.33^{+0.42}_{-0.05}$
17	J1640 + 2224	3.16	2.8e-21	175.5	$0.29^{+0.37}_{-0.04}$
18	J1643 – 1224	4.62	1.8e-20	147.0	$0.14^{+0.15}_{-0.02}$
19	J1708 – 3506	4.51	1.1e-20	149.1	$0.19^{+0.22}_{-0.03}$
20	J1713 + 0747	4.57	8.5e-21	67.8	$0.32^{+0.42}_{-0.05}$
21	J1751 – 2857	3.91	1.1e-20	110.7	$0.23^{+0.27}_{-0.03}$
22	J1806 + 2819	15.08	3.8e-20	43.9	$0.29^{+0.36}_{-0.04}$
23	J1824 – 0621	3.23	9.1e-21	100.9	$0.34^{+0.45}_{-0.05}$
24	J1824 + 1014	4.07	5.4e-21	82.6	$0.31^{+0.40}_{-0.05}$
25	J1825 – 0319	4.55	6.8e-21	52.6	$0.21^{+0.24}_{-0.03}$
26	J1828 + 0625	3.63	4.7e-21	77.9	$0.32^{+0.41}_{-0.05}$
27	J1844 + 0115	4.19	1.1e-20	50.6	$0.16^{+0.18}_{-0.02}$
28	J1850 + 0124	3.56	1.1e-20	84.9	$0.29^{+0.36}_{-0.04}$
29	J1853 + 1303	4.09	8.7e-21	115.7	$0.28^{+0.35}_{-0.04}$
30	J1855 – 1436	3.59	1.1e-20	61.5	$0.31^{+0.40}_{-0.05}$
31	J1858 – 2216	2.38	3.8e-21	46.1	$0.25^{+0.30}_{-0.04}$
32	J1908 + 0128	4.70	5.3e-20	84.2	$0.34^{+0.44}_{-0.05}$
33	J1910 + 1256	4.98	9.7e-21	58.5	$0.22^{+0.27}_{-0.03}$
34	J1913 + 0618	5.03	9.6e-21	67.7	$0.33^{+0.43}_{-0.05}$
35	J1921 + 1929	2.65	3.8e-20	39.6	$0.30^{+0.37}_{-0.04}$
36	J1930 + 2441	5.77	8.7e-21	76.4	$0.27^{+0.33}_{-0.04}$
37	J1935 + 1726	4.20	*	90.8	$0.26^{+0.31}_{-0.04}$
38	J1955 + 2908	6.13	3.0e-20	117.3	$0.21^{+0.25}_{-0.03}$
39	J2019 + 2425	3.93	7.0e-21	76.5	$0.36^{+0.49}_{-0.06}$
40	J2033 + 1734	5.95	1.1e-20	56.3	$0.22^{+0.26}_{-0.03}$
41	J2042 + 0246	4.53	1.4e-20	77.2	$0.22^{+0.26}_{-0.03}$
42	J2229 + 2643	2.98	1.5e-21	93.0	$0.14^{+0.16}_{-0.02}$
43	J2234 + 0611	3.58	1.2e-20	32.0	$0.22^{+0.26}_{-0.03}$
44	J2302 + 4442	5.19	1.4e-20	125.9	$0.34^{+0.45}_{-0.05}$

Table 3. The estimated Galactic rates and numbers of the resulting MSPs for the CCSN and AIC channels with different values of CE ejection parameters, in which we adopt metallicity $Z = 0.02$ and a constant star-formation rate of $5 M_{\odot}\text{yr}^{-1}$ in our Galaxy. Notes: $\alpha_{\text{CE}}\lambda$ = CE ejection parameter; ν_{MSP} = Galactic rates of MSPs; Number = Expected number of resulting MSPs in the Galaxy.

Channels	$\alpha_{\text{CE}}\lambda$	ν_{MSP} (10^{-5}yr^{-1})	Number (10^5)
The CCSN channel	1.0	4.0	4.8
The CCSN channel	1.5	7.1	8.5
The AIC channel	1.0	2.1	2.5
The AIC channel	1.5	3.2	3.8